Numerical Study of Li Diffusion in Polycrystalline $LiCoO_2$

Shunsuke Yamakawa[a, c, *], Hisatsugu Yamasaki[b], Toshiyuki Koyama[c], and Ryoji Asahi[a]

[a]Toyota Central R&D Labs., Inc., Nagakute, Aichi 480-1192, Japan

[b]Toyota Motor Corporation, Susono, Shizuoka 410-1193, Japan

[c]Graduate School of Engineering, Nagoya Institute of Technology, Nagoya, Aichi 466-8555, Japan

∗Corresponding author

Phone: +81-561-71-7127

Fax: +81-561-63-5258

E-mail: e1044@mosk.tytlabs.co.jp

Abstract

Layered Li transition metal oxides are widely used as active materials for the positive electrode of Li-ion rechargeable batteries, where intercalation of Li in the metal oxide is a fundamental phenomenon that determines the performance of the batteries. The intercalation process is significantly affected by the crystal anisotropy and grain boundaries, particularly for all-solid-state thin film batteries. Therefore, to improve the batteries, a thorough understanding of the intercalation process on the nanometer length scale is essential. To this end, we have proposed phase-field models for calculating the relation between the realistic polycrystalline microstructure and the apparent Li diffusion coefficient. A crystallographic orientation was randomly allocated to each crystal grain in a two-dimensional polycrystalline microstructure. The simulation results show that the apparent Li diffusivity is sensitive to the diffusivity of the grain boundaries, the spatial distribution of the crystal orientation for each grain, and the grain size. The diffusivity of a small-grained structure is determined by the properties of the grain boundary. On the other hand, the diffusivity of a large-grained structure depends considerably on the relative orientation angle between neighboring grains, even when the Li conductivity of the grain boundary is large.

Keywords: phase-field model; Li-ion rechargeable battery; intercalation process; grain boundary diffusion; polycrystalline microstructure

Highlights:

- 2D models with randomly oriented microstructures and various grain sizes are employed.
- The grain boundary (GB) is modeled as a thin layer between grains.
- The relative orientation angle between neighboring grains affects Li diffusivity.
- The diffusivity of a small-grained structure is determined by the properties of the GB.
- The influences of the GB properties and the orientation angle can be evaluated separately.

1. Introduction

Layered Li transition metal oxides are widely used as active materials for Li ion rechargeable batteries [1]. The extraction of Li ions from and the insertion of Li ions into a layered cobalt dioxide matrix [2-4] are fundamental phenomena that determine the battery performance [5]. This structure provides two-dimensional (2D) Li diffusion paths, which allows topotactic electrochemical reactions to occur for high-power applications. The self-diffusion coefficient of Li in Li_xCoO_2 (D_{self}) has been investigated using both theoretical and experimental approaches [6-8]. The value of D_{self} estimated from muon-spin spectroscopy [6] is in the range from 1×10^{-10} to 1×10^{-9} cm^2/s for Li_xCoO_2 ($0.5 < x < 0.8$) at a temperature of 300 K, which is in good agreement with the value calculated using a first-principles method [8]. On the other hand, the chemical diffusion coefficient (D_{chem}), which is evaluated by electrochemical measurements, varies from 1×10^{-12} to 1×10^{-10} cm^2/s [9, 10] for (104)-textured thin films, so that grains with their (104) planes parallel to the Li transport direction facilitate the Li transport [11]. It is known that D_{chem} can be expressed as the product of D_{self} and a thermodynamic factor (ω). Since the binary solution of Li vacancies in the 2D layer is not ideal, the value of ω must be larger than 1 for a wide range of Li concentrations. Therefore, D_{chem} is expected to be larger than D_{self}, which contradicts the experimental data. The transport properties of Li seem to be limited by microstructural inhomogeneities such as the crystal anisotropy, grain size, and grain boundaries. In a commercial Li-ion battery, the electrolyte that intrudes into pores within a secondary particle may provide short-circuit transport paths for Li. Nevertheless, experimental observation [12] has shown that secondary particle contains numerous grain boundaries, which means that a primary particle within a secondary

particle is not fully isolated and the surface does not fully expose to the electrolyte. On the other hand, in the case of the all-solid-state battery with a flat thin-film electrode, since most crystal grains do not directly touch solid electrolyte particles, the inter-granular diffusion between crystal grains plays a crucial role in the Li transport. Therefore, to improve the batteries, a thorough understanding of the intercalation process on the nanometer length scale is essential. This paper focuses on gaining a quantitative understanding of the relation between the morphology of the microstructure and the Li diffusivity using numerical simulation techniques.

Most previously reported numerical simulations [13-15] have adopted several assumptions about the anisotropic Li intercalation process, such as an isotropic grain model and linear Fickian diffusion of Li inside the grains. In these models, because the influence of the polycrystalline anisotropic microstructure on the Li mobility was taken into account through apparent diffusion coefficients, the reaction and the diffusion process of the practical battery electrode were greatly simplified. Consequently, such models could fail to capture important aspects of the charging or discharging dynamics in an essentially anisotropic inhomogeneous medium. It can easily be imagined that a linked approach for simultaneously modeling the microstructure and the transport will be indispensable, because microstructural modeling that does not consider transport cannot identify optimal transport properties for a particular application. The phase-field method has recently attracted increasing attention as a promising technique [16, 17] for calculating the morphological characteristics through microstructural evolution on a nanometer length scale. The method has also been applied to describe Li diffusion in a phase-separated system [18, 19] and to simulate the anisotropic electrochemical strain microscopy (ESM) response of polycrystalline $LiCoO_2$ [20]. In this paper, an integrated

computational approach for simulating the morphology of the polycrystalline microstructure and evaluating the corresponding apparent Li diffusion coefficient (D_{app}) in the microstructure is proposed. A realistic 2D polycrystalline model has been generated from the phase-field simulations. A crystallographic orientation was randomly allocated to each crystal grain. In this model, the grain boundary (GB) was treated as a thin layer between two crystal grains. D_{app} was obtained from the temporal evolution of the Li concentration by using the Cahn-Hilliard diffusion equation [21], which treats non-Fickian Li diffusion in combination with the anisotropic self-diffusion tensor. A phenomenological constitutive relation between Li conductivity and quantitative microstructural features such as average grain size and crystallographic orientation was directly provided from the simulation results.

The outline of this paper is as follows. In Sec. 2, the main characteristics of the simulation methods used to model the polycrystalline microstructure, the Li diffusion properties, and their integration are described. In Sec. 3, practical applications are illustrated using a 2D system. The dependence of D_{app} on the various grain sizes and crystal orientation angles between neighboring grains in the microstructure models is discussed. We also used the phase-field model to study the Li segregation in polycrystalline Li_xCoO_2 thin film during the discharge process at a constant current. The conclusions are given in Sec. 4.

2. Calculation Method

2.1 Cahn-Hilliard Diffusion Equation

In order to represent the isotropic Li diffusion, we introduce the Cahn-Hilliard diffusion equation expressed in the following form:

$$\frac{\partial c}{\partial t} = \nabla\left[\frac{c(1-c)D_{\text{self}}}{RT}\nabla\mu\right], \quad (1)$$

where c is the local concentration of Li normalized by the maximum Li concentration ($c_{\text{Li}}^{\max}$), so that it is nondimensional and only takes values between 0 and 1. D_{self} is the self-diffusion coefficient of Li. R and T are the gas constant and the absolute temperature, and μ represents the diffusion potential of Li, which is defined as the functional derivative of the total chemical free energy (G_{sys}) with respect to local concentration:

$$\mu = \frac{\delta G_{\text{sys}}}{\delta c}. \quad (2)$$

G_{sys} is expressed as the volume integral of the local chemical free energy (G_{m}) and the gradient energy term over the entire system:

$$G_{\text{sys}} = \frac{1}{V}\int\left[G_{\text{m}} + \frac{\kappa}{2}(\nabla c)^2\right]dV, \quad (3)$$

where G_{m} is the Gibbs energy of the uniform binary solution in the Li-vacancy system and κ is the gradient energy coefficient, which is estimated from the interaction parameters obtained by fitting the Gibbs energy function [22] to the mixing enthalpy of the disordered solution. We employed the mixing enthalpy value estimated from the first-principles calculation given in Refs. [23] and [24]. By substituting Eqs. (2) and (3) into Eq. (1), it can be rewritten as

$$\frac{\partial c}{\partial t} = \nabla\left[\frac{c(1-c)D_{\text{self}}}{RT}\nabla\left(\frac{\partial G_{\text{m}}}{\partial c} - \kappa\nabla^2 c\right)\right]. \quad (4)$$

Here, $\partial G_{\text{m}}/\partial c$ is evaluated by utilizing the electrochemical potential:

$$\frac{\partial G_{\text{m}}}{\partial c} = -n_{\text{Li}}F\left(U_{\text{LiCoO}_2} - U_{\text{ave}}\right), \quad (5)$$

where n_{Li} is the number of electrons in the charge-transfer reaction, *i.e.*, $n_{Li} = 1$ in $Li^+ + e^- = Li$, and F is Faraday's constant. U_{LiCoO_2} is the equilibrium potential of $LiCoO_2$, which is evaluated by using Eq. (6) in Ref. [25]

$$c = \sum_{i=1}^{n} \frac{c_{\max,i}}{1+\exp\left[\frac{F}{\xi RT}\left(U_{LiCoO_2} - U_i^0\right)\right]}. \quad (6)$$

It is noted that U_{LiCoO_2} is given as a function of c. The parameters $c_{\max,i}$, ξ, and U_i^0 were determined by fitting the function to experimental open-circuit potential data [25]. The average potential (U_{ave}) is given by the expression

$$U_{ave} = (G_{LiCoO_2} - G_{CoO_2} - G_{Li}) / (-n_{Li}F). \quad (7)$$

To verify the accuracy of the present phase-field model, we used it to estimate the thermodynamic factor (ω) defined as the ratio of D_{chem} to the given D_{self} in homogeneous $LiCoO_2$. A one-dimensional model with an electrode thickness of 1 μm was employed to mimic the potentiostatic intermittent titration technique (PITT) [26]. The temperature was set at 300.15 K. A potential step of 2 mV was applied, and the current as a function of time was recorded. D_{chem} was calculated from the time dependence of the current. The accuracy of this simulation program is verified through the comparison of the calculated ω with the experimental result [10], as shown in Fig. 1. It can be seen that ω exhibits considerable variations near the composition of $\delta = 0.5$ ($Li_{0.5}CoO_2$), which are induced by an increase in the degree of Li-vacancy ordering [27]. The simulated result was overall in good agreement with the measured result [10], legitimating the modeling and the parameters used for the simulation.

2.2 Li Diffusion in Polycrystalline Material

Figure 2 shows the microstructural features considered in this model. Eq. (4) can be rewritten in a formulation using the anisotropic diffusion tensor in order to represent Li diffusion within a $LiCoO_2$ grain:

$$\frac{\partial c}{\partial t}=\frac{\partial}{\partial x}\left[\frac{c(1-c)}{RT}\left(D_{\mathrm{xx}}\frac{\partial \mu}{\partial x}+D_{\mathrm{xy}}\frac{\partial \mu}{\partial y}\right)\right]+\frac{\partial}{\partial y}\left[\frac{c(1-c)}{RT}\left(D_{\mathrm{yx}}\frac{\partial \mu}{\partial x}+D_{\mathrm{yy}}\frac{\partial \mu}{\partial y}\right)\right], \quad (8)$$

$$\mathbf{D}=\begin{bmatrix} D_{xx} & D_{xy} \\ D_{yx} & D_{yy} \end{bmatrix}=\begin{bmatrix} D_{\mathrm{self}}\sin^2\theta+D_{\mathrm{self\_}c\,\mathrm{axis}}\cos^2\theta & \left(D_{\mathrm{self}}-D_{\mathrm{self\_}c\,\mathrm{axis}}\right)\sin\theta\cos\theta \\ \left(D_{\mathrm{self}}-D_{\mathrm{self\_}c\,\mathrm{axis}}\right)\sin\theta\cos\theta & D_{\mathrm{self}}\cos^2\theta+D_{\mathrm{self\_}c\,\mathrm{axis}}\sin^2\theta \end{bmatrix}, \quad (9)$$

where $D_{\mathrm{self\_}c\,\mathrm{axis}}$ is the self-diffusion coefficient along the crystallographic *c*-axis direction and θ is the angle between the global Li transport direction and the crystallographic basal plane of the hexagonal $LiCoO_2$. The GB is assumed to be a thin layer between neighboring grains [28]. In the 2D GB model, a change in the Li concentration in the GB is calculated by the following equations, where the coefficient β is introduced to represent that the Li diffusivity along the GB core and that across the interface between a grain and a GB layer are different from the diffusivity within the grain:

$$\frac{\partial c}{\partial t}=-\frac{1}{h}\left(J_{i=h/2}-J_{i=-h/2}\right)+\frac{\partial}{\partial s}\left[\frac{c(1-c)\beta D_{\mathrm{self}}}{RT}\frac{\partial \mu}{\partial s}\right]. \quad (10)$$

Here, *h* is the GB width, $J_{i=h/2\,\mathrm{or}\,-h/2}$ denotes the flux of Li across the interface between a grain and a GB layer, and *s* is the direction along the GB. Calculations were performed for such an inhomogeneous system consisting of the grain and the GB by solving the two types of differential equations, Eqs. (8) and (10), simultaneously.

2.3 Polycrystalline Microstructure

In order to quantitatively discuss the relation between the polycrystalline

microstructure and the Li diffusivity, we prepared various types of polycrystalline microstructures, as shown in Fig. 3. The microstructures were obtained by using the multi-phase-field algorithm [29] under periodic boundary conditions. The ideal grain growth for a system was simulated under the assumption that the GB energy and the GB mobility are isotropic. The orientation angle θ assigned to each grain is thus expressed by

$$\theta = m\Delta\theta, \quad (11)$$

where $\Delta\theta$ is defined as 180° divided by the total number of grains (N_{gb}). The variable m, which is an integer between zero and N_{gb}, is randomly assigned to each crystal grain. When θ is zero or 180°, the c-axis of the hexagonal $LiCoO_2$ crystallite is perpendicular to the global Li transport direction. The diameter of an irregularly shaped grain was calculated as that of the circle with the equivalent area. In the following section, the grain size in the polycrystalline model is represented by the ratio of the mean grain diameter to the length of the simulation region (L).

2.4 Numerical Calculation

2D numerical calculations were performed by using the finite volume method with the explicit Euler method. The boundary conditions are listed in Table 1. The temperature was 300.15 K, the grid spacing was 0.02 μm, and the simulation region was a square with a size of 4.0 × 4.0 μm^2. Specifically, a finer grid spacing near the GBs was used so that the GB surface could be well represented. The parameters used in the numerical calculation are listed in Table 2. Taking into account the experimental Li conductivities obtained using the PITT method for thin films with (003) and (104) preferred orientations [10], $D_{self\_c\,axis}$ is assumed to be 100 times smaller than the D_{self}

value.

The temporal evolution of the Li concentration in the microstructure induced by a concentration gradient along the *y*-axis was calculated numerically, as shown in Fig. 4. The initial concentration of Li in the microstructure was 0.6, and the Li concentration at $y = L$ was fixed to 0.61. Once dc/dt is obtained, D_{app} of Li in the calculation region can be analytically evaluated using the following equation [26]:

$$D_{app} = -\frac{d\ln(dc/dt)}{dt}\frac{4L^2}{\pi^2}, \text{ if } t >> L^2/D_{app}. \quad (12)$$

where L corresponds to the macroscopic Li diffusion length. In the isotropic diffusion system, where Eq. (1) holds, D_{app} corresponds to the chemical diffusion coefficient, and the value is greater than or equal to D_{self}.

When the electrochemical reaction is explicitly treated with the purpose of investigating the degree of Li segregation under realistic discharge conditions, the Butler-Volmer equation [13] is incorporated in the model to describe the charge-transfer reaction occurring across the $LiCoO_2$-electrolyte interface at $y = L$. The total Li intercalation flux per unit area (J_{total}) is then defined in the following expression:

$$J_{total} = \frac{1}{L}\int J(x, y = L)dx, \quad (13)$$

$$J(x, y = L) = k\left\{\exp\left[\frac{\alpha_a n_{Li} F}{RT}\left(\phi - U_{LiCoO_2}\right)\right] - \exp\left[-\frac{\alpha_c n_{Li} F}{RT}\left(\phi - U_{LiCoO_2}\right)\right]\right\}, \quad (14)$$

$$k = k_0 \cos\theta\left(c_{Li}^{max} - c_{Li}\right)^{\alpha_a}\left(c_{Li}\right)^{\alpha_c}\left(c_{Li^+}\right)^{\alpha_a}, \quad (15)$$

where ϕ is the electrode potential and k is the kinetic rate of the electrochemical reaction, which depends on the angle between the basal plane of $LiCoO_2$ and the tangent line of the interface between $LiCoO_2$ and the electrolyte. Here c_{Li} and c_{Li^+} are the Li concentrations in $LiCoO_2$ and the electrolyte, respectively, and α_a and α_c are the anodic

and cathodic transfer coefficients, respectively. In addition, k_0 and c_{Li}^{max} are the kinetic rate constant of the electrochemical reaction and the maximum Li concentration in $LiCoO_2$. The values of these parameters used for the simulations are also listed in Table 2. The equilibrium potential function of $LiCoO_2$ is the same as in Eq. (6). The current density (I) for this reaction is expressed as $I = J_{total}/F$, and the value is fixed at 0.276 mA/cm^2. To obtain the converged ϕ value for each individual time step, the Newton-Raphson method is employed. In addition, the potential distribution in $LiCoO_2$ and the electrolyte and the mass transport of Li ions in the electrolyte are calculated by using the conventional formulation given in [13].

3. Results and Discussion

The dependence of D_{app} on the grain size and on the manner in which the crystal orientation was assigned to each grain was investigated. We defined the mean orientation angle (θ_{mean}) by the following equation:

$$\theta_{mean} = 90 - \sum_{n_y=1}^{n_y=n_{y\_max}} \sum_{n_x=1}^{n_x=n_{x\_max}} \left| 90 - \theta\left(n_x, n_y\right) \right| / \left(n_{x\_max} \times n_{y\_max}\right), \quad (16)$$

where n_{x_max} and n_{y_max} mean the numbers of grid points along the x-axis and y-axis, respectively, in the numerical simulation region. For this assignment method, θ_{mean} approaches 45° as the number of grains increases. The D_{app} value of the single-crystalline model with $\theta = 45°$ was about 3.6×10^{-9} cm^2/s. Figure 5 shows D_{app} as a function of the normalized grain size (d_{mean}/L) for simulations using two different values of β. In the case of $\beta = 1.0$, Li is assumed to diffuse in the GB with the same D_{self} value as that in the inner grain. At a glance, all of the D_{app} values corresponding to the polycrystalline models are smaller than those of the single-crystalline model with θ

= 45°. A decrease in the grain size leads to an increase in D_{app}. When we compare the calculation results for β = 0.01, in contrast with those for β = 1.0, a decrease in the grain size did not directly lead to an increase in D_{app}. In this case, the GB seems to have a blocking character for Li diffusion. The Li transport involving the GB network is notably affected for a large value of β; the inverse proportionality between D_{app} and the grain size is mainly due to the Li diffusion process utilizing a kind of a channeling through the GB network.

Another important feature shown in Fig. 5 is that there are remarkable variations in D_{app} even when d_{mean} is the same. These variations uniquely depend on the assignment of the orientation angle to each grain. D_{app} is plotted against θ_{mean} in Fig. 6. The symbols corresponding to d_{mean}/L values of 0.3 or 0.4 show that D_{app} slightly decreases as θ_{mean} increases. Since a θ value of 90° corresponds to a crystallographic *c*-axis parallel to the Li transport direction, this tendency is reasonable. However, since the variation of D_{app} is still wide even with the same θ_{mean} value, it is hard to estimate the value of D_{app} from only the value of θ_{mean}. In fact, the influence of the connectivity of the conduction path between the crystal grains is not represented by the θ_{mean} value. To address this, the area-averaged value was evaluated using the following equation to take into account the relative orientation between neighboring grains:

$$\theta_{\text{relative}} = 90 - \sum_{n_y=1}^{n_y=n_{y\_\max}} \left| \sum_{n_x=1}^{n_x=n_{x\_\max}} \left\{ 90 - \theta\left(n_x, n_y\right) \right\} \right| / \left(n_{x\_\max} \times n_{y\_\max} \right). \quad (17)$$

In this case, the summation takes into account the different signs of θ instead of the absolute value. In Fig. 7, D_{app} is plotted against the mean value of the relative orientation angle (θ_{relative}). As shown in Fig. 7, θ_{relative} shows a clear correlation with D_{app}. Large θ_{relative} values mean that most interfaces parallel to the *y*-axis have such a

character that the signs of the angles for the two neighboring grains that sandwich the interface are opposite. When all the GBs parallel to the *y*-axis are so-called twin boundaries, the $\theta_{relative}$ value reaches 90°. In this case, the flux of Li is restricted by the region near the GBs because of the disconnectedness of the 2D accessible path for Li diffusion. The good correlation between $\theta_{relative}$ and D_{app} implies that the characteristics of the GBs parallel to the Li transport direction significantly affect the Li diffusivity. Recently, experimental observation has revealed that the high-coincidence twin boundary stably exists in $LiCoO_2$ thin films [30]. Therefore, it is thought that the restriction of Li flux by the disconnectedness of the 2D accessible path described in this paper occurs in the actual polycrystalline $LiCoO_2$ film. Moreover, the D_{app} values corresponding to the d_{mean}/L value of 0.05 for $\beta = 1.0$ shown in Fig. 7 (b) are somewhat larger than the value expected from the results for the d_{mean}/L values of 0.3 and 0.4. This is mainly because the Li flux in microstructures with such a small grain size and such good conductive GBs is determined by the GB diffusion. When GB diffusivity is poor, e.g., when $\beta = 0.01$, the D_{app} value corresponding to $d_{mean}/L = 0.05$ is in good agreement with the one predicted using other d_{mean}/L values, as shown in Fig. 7 (a). Consequently, both the GB diffusivity and the relative orientation angle between neighboring grains affect Li diffusivity. When the grain size is significantly small, the Li diffusivity is probably rate-determined by the GB diffusion, since there are a number of ways to assign the crystal orientation for each grain such that the resultant $\theta_{relative}$ values are almost the same among the models generated for simulations. On the other hand, the diffusivity of a large-grained structure model depends considerably on the relative orientation angle between neighboring grains, even when the Li conductivity of the GB is large, resulting in the variations of D_{app}. When the electrode size is quite large, such a

local inhomogeneity is fully averaged. However, in the case of thin film electrodes, d_{mean} relative to the electrode thickness is not very large. Therefore, the evaluation of d_{mean}/L is useful for obtaining the appropriate electrode microstructure. Once we can experimentally evaluate the grain size relative to the electrode size from a 2D image, we can roughly estimate the possible in-plane variation in electrode performance in comparison with d_{mean}/L squared.

These results were also used to obtain the ratio of the D_{app} of the microstructure with randomly oriented grains relative to that of the microstructure in which the grains are oriented with $\theta = 0°$. Figure 8 plots this ratio against the grain size. The ratio decreased as the grain size increased, and the ratio varied within the range of 0.05 to 0.45. In addition, because the ratio behaved similarly for both $\beta = 1$ and $\beta = 0.01$, it follows that the influences of the GB diffusivity and $\theta_{relative}$ can be evaluated separately. The experimental value of the ionic conductivity obtained using the electron blocking method with a randomly oriented sample is between the conductivities for the (003) and (104) orientations of $LiCoO_2$ [10]. Furthermore, the ratio of the conductivity of the (104) oriented film to that of the randomly oriented sample is roughly 0.3 for a composition of $Li_{0.65}CoO_2$ [10]. Hence, the calculated results are consistent with the experimental results. On the other hand, the D_{app} with $\beta = 1$ is still large in comparison with the experimental D_{chem} of the PLD film measured by PITT, which varied in the range from 10^{-12} to 10^{-10} cm^2/s [9, 10]. To obtain a good match between the value of D_{app} and the measured value, an extremely low Li GB diffusivity is suggested. Recently, the results of first-principles calculations [30] have shown that the activation energy of Li diffusion near the high-coincidence twin boundary is higher than that of the crystal interior. This type of GB seems to act as a prevention factor for Li diffusion.

Contrary to these expectations, recent ESM results reported a high Li mobility near certain GBs [31]. Therefore, we cannot find conclusive evidence to clarify the actual GB diffusivity.

Another important aspect of the charging or discharging dynamics is the Li segregation in the polycrystalline $LiCoO_2$ thin film induced by the microstructural anisotropy. To investigate that, we used the phase-field model in combination with the electrochemical model. Figure 9 shows the change in the Li concentration in polycrystalline $LiCoO_2$ during the discharge process at a constant current. Li tends to rapidly diffuse in the direction along the basal plane. As shown in Fig. 9, more remarkable Li segregation was induced when d_{mean}/L was larger than 0.1. The simulation results also show that the Li segregation was enhanced by decreases in the GB diffusivity. When the grain size relative to the $LiCoO_2$ thickness is small, such as when $d_{mean}/L = 0.05$, the existence of several possible diffusion paths leads to a decrease in the degree of Li segregation. These results suggest that Li piles up in one grain when an intergranular angle mismatch is large or when the GB diffusivity is poor, while the assumption of isotropic diffusion is valid for strictly limited cases.

4. Conclusions

We have used the phase-field model to investigate Li diffusion in polycrystalline Li_xCoO_2 randomly oriented on a nanometer length scale. The simulation results demonstrated that Li diffusivity in anisotropic material was determined by the balance between several basic characteristics related to the microstructure, such as the GB, the crystallographic orientation, and the grain size. The diffusivity of the small-grained structure is determined by the GB properties. On the other hand, when the grain size is

large, the variation in the mean relative orientation angle between neighboring grains increases. Consequently, the diffusivity of the large-grained structure varies considerably even when the Li conductivity of the GB is large. It is possible that the diffusivity of a randomly oriented and large-grained microstructure will be one order of magnitude smaller than that of the $\theta = 0°$ textured microstructure. This work has provided a clue to understanding the Li transport properties such as those in a thin film electrode for an all-solid-state battery. Since observable phenomena only represent consequences of the multistep process, it is difficult to separately evaluate the role of each basic step. Therefore, the integrated computational approach that simultaneously simulates the microstructure and evaluates the transport properties presented here may help to obtain a quantitative understanding of each basic step of the Li transport process.

References

[1] J.-M. Tarascon, M. Armand, Nature 414 (2001) 359-367.

[2] K. Mizushima, P.C. Jones, P.J. Wiseman, J.B. Goodenough, Mat. Res. Bull. 15 (1980) 783-789.

[3] E. Plichta, M. Salomon, S. Slane, M. Uchiyama, D. Chua, W.B. Ebner, H.W. Lin, J. Power Sources 21 (1987) 25-31.

[4] J.J. Auborn, Y.L. Barberio, J. Electrochem. Soc. 134 (1987) 638-641.

[5] E. Antolini, Solid State Ionics 170 (2004) 159-171.

[6] J. Sugiyama, K. Mukai, Y. Ikedo, H. Nozaki, M. Månsson, I. Watanabe, Phys. Rev. Lett. 103 (2009) 147601.

[7] M. Okubo, Y. Tanaka, H. Zhou, T. Kudo, I. Honma, J. Phys. Chem. B 113 (2009) 2840-2847.

[8] A. Van der Ven, G. Ceder, M. Asta, P.D. Tepesch, Phys. Rev. B 64 (2001) 184307.

[9] H. Xia, L. Lu, Electrochim. Acta 52 (2007) 7014-7021.

[10] J. Xie, N. Imanishi, T. Matsumura, A. Hirano, M. Matsumura, Y. Takeda, O. Yamamoto, Solid State Ionics 179 (2008) 362-370.

[11] J.B. Bates, N.J. Dudney, B.J. Neudecker, F.X. Hart, H.P. Jun, S.A. Hackney, J. Electrochem. Soc. 147 (2000) 59-70.

[12] J.R. Wilson, J.S. Cronin, S.A. Barnett, S.J. Harris, J. Power Sources 196 (2011) 3443-3447.

[13] P. Ramadass, B. Haran, R. White, B.N. Popov, J. Power Sources 123 (2003) 230-240.

[14] S. Santhanagopalan, Q. Guo, P. Ramadass, R.E. White, J. Power Sources 156 (2006) 620-628.

[15] S. Santhanagopalan, Q. Guo, R.E. White, J. Electrochem. Soc. 154 (2007) A198-A206.

[16] L.Q. Chen, Annu. Rev. Mater. Res. 32 (2002) 113-140.

[17] T. Koyama, Sci. Technol. Adv. Mater. 9 (2008) 013006.

[18] B.C. Han, A. Van der Ven, D. Morgan, G. Ceder, Electrochim. Acta 49 (2004) 4691-4699.

[19] G.K. Singh, G. Ceder, M.Z. Bazant, Electrochim. Acta 53 (2008) 7599-7613.

[20] D-W. Chung, N. Balke, S.V. Kalinin, R.E. Garćia, J. Electrochem. Soc. 158 (2011) A1083-A1089.

[21] J.W. Cahn, J.E. Hilliard, J. Chem. Phys. 28 (1958) 258-267.

[22] T. Abe, T. Koyama, CALPHAD 35 (2011) 209-218.

[23] A. Van der Ven, M.K. Aydinol, G. Ceder, G. Kresse, J. Hafner, Phys. Rev. B 58 (1998) 2975-2987.

[24] C. Wolverton, A. Zunger, Phys. Rev. B 57 (1998) 2242-2252.

[25] Q. Zhang, Q. Guo, R.E. White, J. Electrochem. Soc. 153 (2006) A301-A309.

[26] C.J. Wen, B.A. Boukamp, R.A. Huggins, W. Weppner, J. Electrochem. Soc. 126 (1979) 2258-2266.

[27] J.N. Reimers, J.R. Dahn, J. Electrochem. Soc. 139 (1992) 2091-2097.

[28] D. Gryaznov, J. Fleig, J. Maier, Solid State Ionics 177 (2006) 1583-1586.

[29] S.G. Kim, D.I. Kim, W.T. Kim, Y.B. Park, Phys. Rev. E 74 (2006) 061605.

[30] C. A. J. Fisher, R. Huang, T. Hitosugi, H. Moriwake, A. Kuwabara, Y. H. Ikuhara, H. Oki, Y. Ikuhara, Nanosci. Nanotechnol. Lett. 4 (2012) 165-168.

[31] N. Balke, S. Jesse, A.N. Morozovska, E. Eliseev, D.W. Chung, Y. Kim, L. Adamczyk, R.E. García, N. Dudney, S.V. Kalinin, Nature Nanotechnol. 5 (2010) 749-754.

Table 1. Boundary conditions.

$x = 0$ and $x = L$	$y = 0$	$y = L$
$c_{x=0} = c_{x=L}$	$\mathbf{n}\cdot\nabla c = 0$	c = constant or J_{total} = constant

Table 2. Parameter values for numerical simulation.

Parameter	Value
Self-diffusion coefficient of Li, D_{self} (in the direction along the basal plane) (cm^2/s)	1×10^{-9} [8]
$D_{self\_c\ axis}$ (in *c*-axis direction) (cm^2/s)	1×10^{-11}
Grain boundary width, *h* (nm)	10.0
Gradient energy coefficient, κ (J m^2/mol)	-4.0×10^{-14}
Kinetic rate constant of the electrochemical reaction, k_0 ($cm^{5/2}/mol^{1/2}$ s)	2.6×10^{-6}
Anodic transfer coefficient, α_a	0.5
Cathodic transfer coefficient, α_c	0.5
Maximum Li concentration, c_{Li}^{max} (mol/cm^3)	0.051555

Figure Captions

FIG. 1. Variation of the thermodynamic factor of Li, which is defined as the ratio of the chemical diffusion coefficient to the self-diffusion coefficient, with composition.

FIG. 2. Schematic illustration of microstructural characteristics treated in this simulation.

FIG. 3. Microstructures with randomly oriented grains and ratios of the mean grain diameter to the length of the simulation region of about (a) 0.05, (b) 0.1, (c) 0.2, (d) 0.3, and (e) 0.4. The orientation angle of each grain is represented by its gray tone.

FIG. 4. Temporal evolution of the mean Li concentration in the simulation region. The concentration gradually becomes close to the concentration supplied at the position of $y = L$. The value of $d\ln(dc/dt)/dt$ becomes constant at times larger than L^2/D_{app}.

FIG. 5. Relation between the apparent diffusion coefficient and the grain size. The D_{app} distribution for each grain size and β value originates from differing ways of assigning the crystal orientation for each grain.

FIG. 6. Relation between the apparent diffusion coefficient and the mean value of the orientation angle θ_{mean} estimated using Eq. (16) for (a) $\beta = 0.01$ and (b) $\beta = 1.0$.

FIG. 7. Relation between the apparent diffusion coefficient and the mean value of the orientation angle $\theta_{\mathrm{relative}}$ estimated using Eq. (17) for (a) $\beta = 0.01$ and (b) $\beta = 1.0$.

FIG. 8. Relation between the grain size and the ratio of the D_{app} value of the microstructure with randomly oriented grains to that of the microstructure in which the grains were oriented with $\theta = 0°$. Open squares and filled circles denote the mean values of the ratio. The ranges of variation of the ratio are shown as error bars.

FIG. 9. Change in Li concentration during a constant-current discharge process. The Li transport direction is parallel to the y-axis. Here c_{mean} indicates the Li composition in Li_xCoO_2 averaged over the entire simulation region. The electrolyte near $LiCoO_2$ is represented by a blue thin layer at $y \geq L$.

FIG. 1.

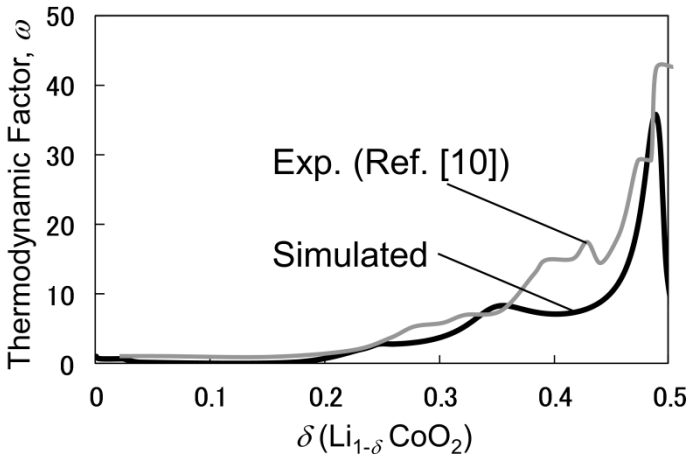
Thermodynamic Factor, ω
50
40
30
20
10
0
0
0.1
0.2
0.3
0.4
0.5
δ (Li1-δ CoO2)
Exp. (Ref. [10])
Simulated

FIG. 2.

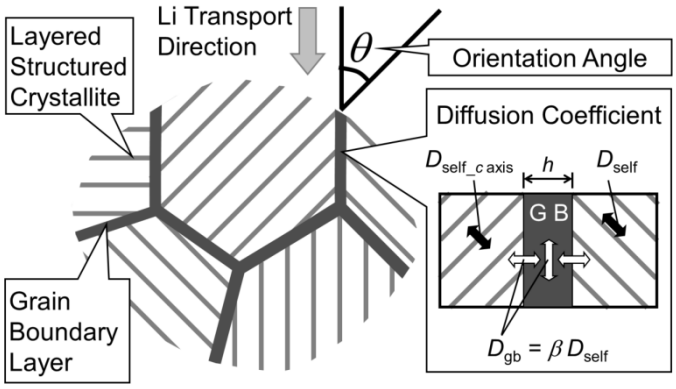
Layered
Structured
Crystallite
Li Transport
Direction
θ
Orientation Angle
Diffusion Coefficient
D self_c axis
h
D self
G B
Grain
Boundary
Layer
D gb = β D self

FIG. 3.

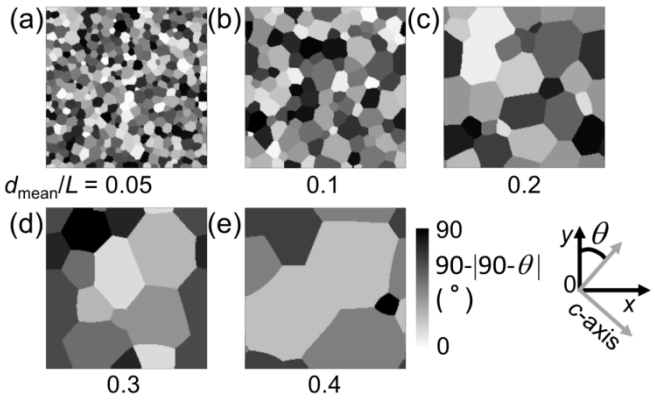

FIG. 4.

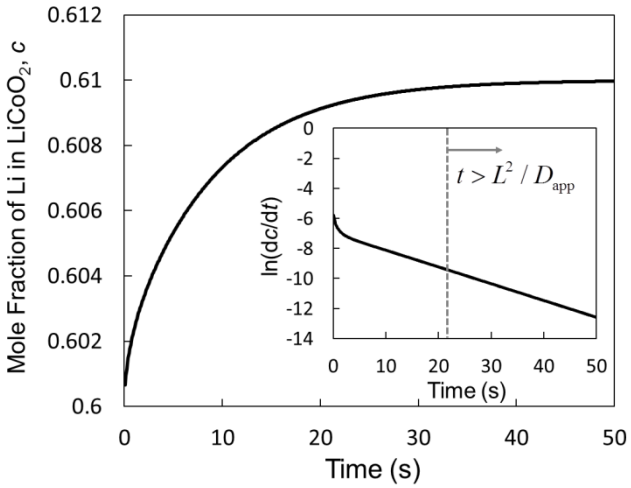
Mole Fraction of Li in $LiCoO_2$, c
0.612
0.61
0.608
0.606
0.604
0.602
0.6
0
10
20
30
40
50
Time (s)
ln(dc/dt)
0
-2
-4
-6
-8
-10
-12
-14
$t > L^2 / D_{app}$
0
10
20
30
40
50
Time (s)

FIG. 5.

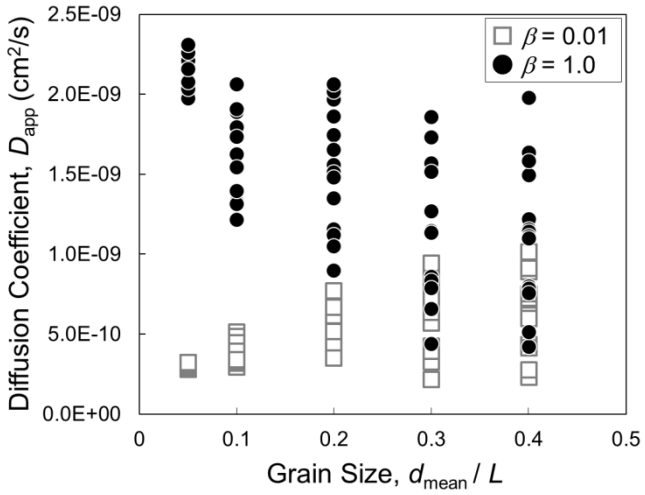
2.5E-09
2.0E-09
1.5E-09
1.0E-09
5.0E-10
0.0E+00
Diffusion Coefficient, D_{app} (cm²/s)
0
0.1
0.2
0.3
0.4
0.5
Grain Size, d_{mean} / L
β = 0.01
β = 1.0

FIG. 6 (a).

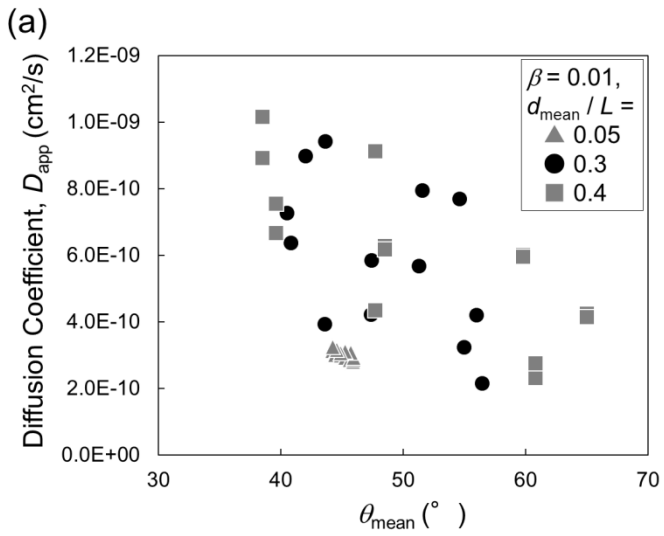
(a)
Diffusion Coefficient, D_{app} (cm^2/s)
1.2E-09
1.0E-09
8.0E-10
6.0E-10
4.0E-10
2.0E-10
0.0E+00
30
40
50
60
70
θ_{mean} (°)
β = 0.01,
d_{mean} / L =
0.05
0.3
0.4

FIG. 6 (b).

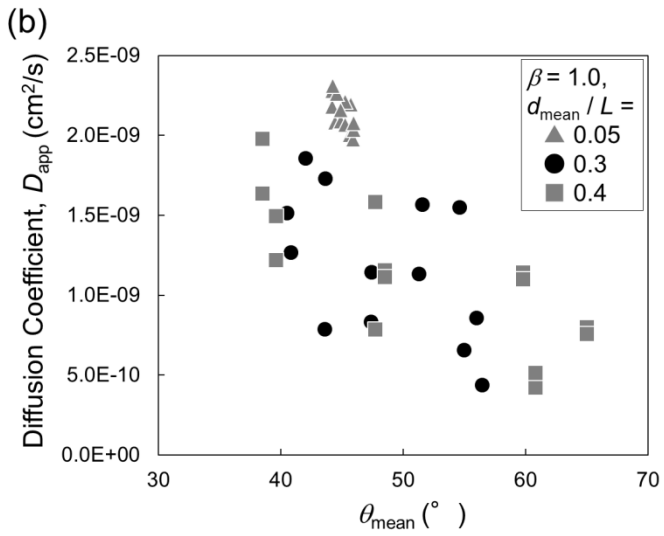
(b)
Diffusion Coefficient, D_{app} (cm^2/s)
2.5E-09
2.0E-09
1.5E-09
1.0E-09
5.0E-10
0.0E+00
30
40
50
60
70
θ_{mean} (°)
β = 1.0,
d_{mean} / L =
0.05
0.3
0.4

FIG. 7 (a).

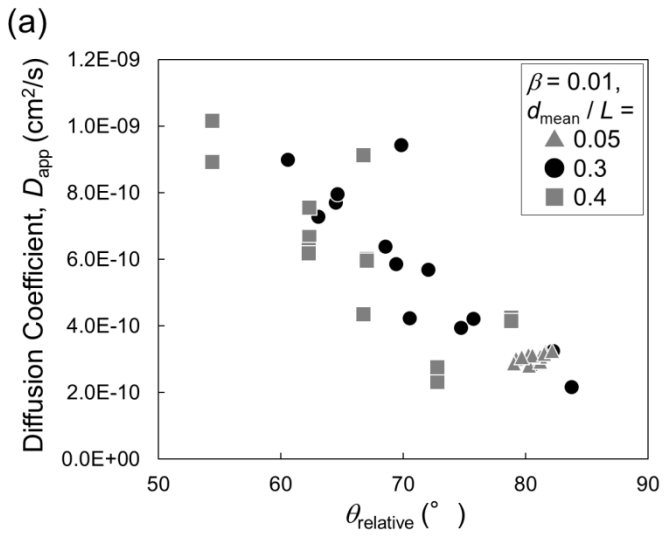
(a)
Diffusion Coefficient, D_{app} (cm^2/s)
1.2E-09
1.0E-09
8.0E-10
6.0E-10
4.0E-10
2.0E-10
0.0E+00
50
60
70
80
90
$\theta_{relative}$ (°)
β = 0.01,
d_{mean} / L =
0.05
0.3
0.4

FIG. 7 (b).

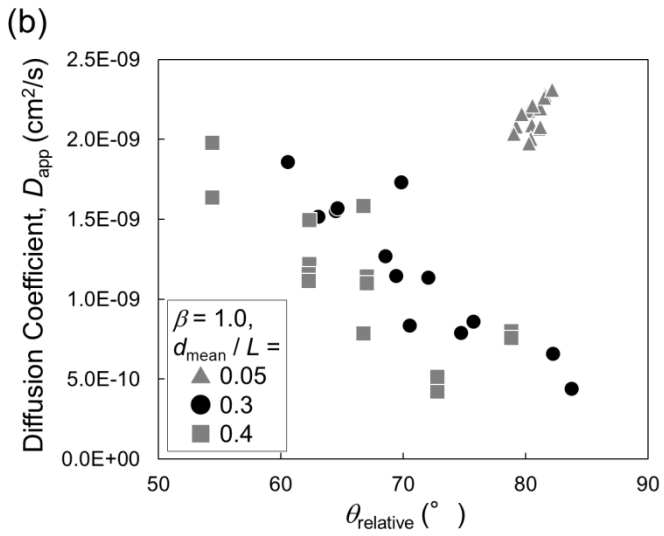
(b)
Diffusion Coefficient, D_{app} (cm^2/s)
2.5E-09
2.0E-09
1.5E-09
1.0E-09
5.0E-10
0.0E+00
50
60
70
80
90
$\theta_{relative}$ (°)
β = 1.0,
d_{mean} / L =
0.05
0.3
0.4

FIG. 8.

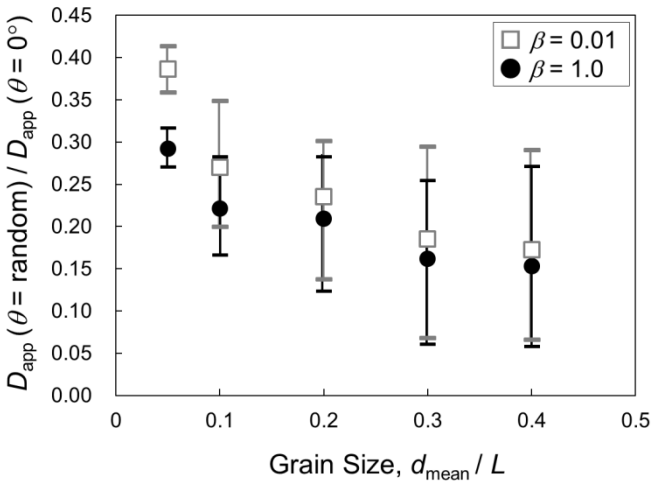
0.45
0.40
0.35
0.30
0.25
0.20
0.15
0.10
0.05
0.00
0
0.1
0.2
0.3
0.4
0.5
β = 0.01
β = 1.0
D_{app} (θ = random) / D_{app} (θ = 0°)
Grain Size, d_{mean} / L

FIG. 9.

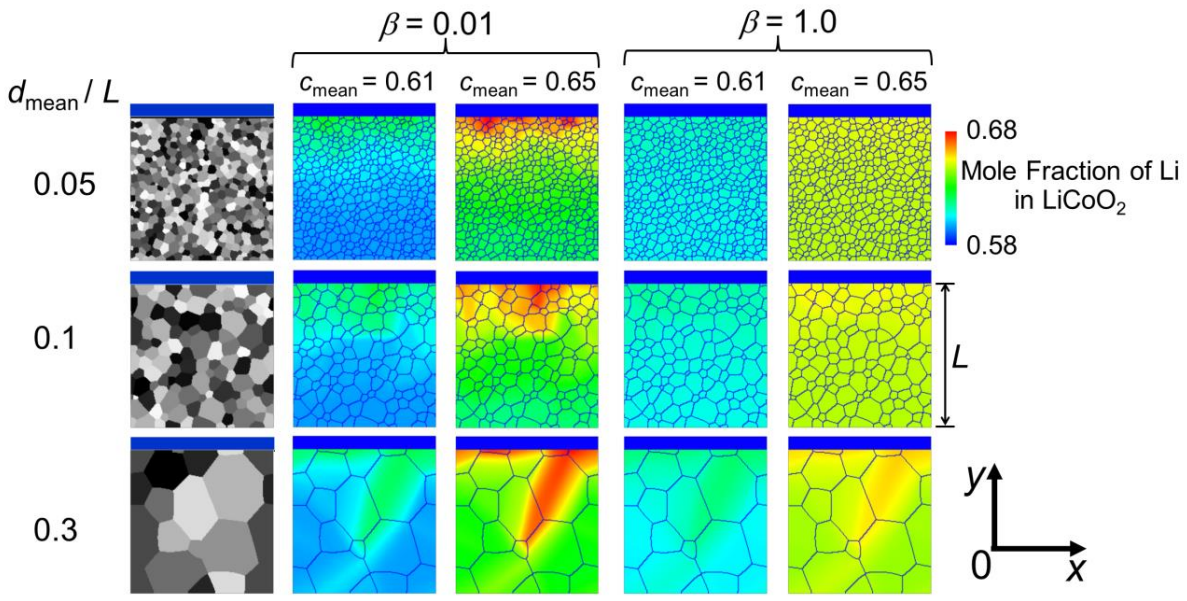
β = 0.01
β = 1.0
c_mean = 0.61
c_mean = 0.65
c_mean = 0.61
c_mean = 0.65
d_mean / L
0.05
0.1
0.3
0.68
Mole Fraction of Li in LiCoO2
0.58
L
y
0
x